Hindawi
Geofluids
Volume 2022, Article ID 6864786, 16 pages
https://doi.org/10.1155/2022/6864786

Research Article

Integrated Geologic Modeling of Fault-Block Reservoir: A Case Study of Ss Oil Field

Zhipeng Xiao,[1] Zhang Wei,[1] Zhengyin Tang,[2] Jianqing Guo,[1] Ruijuan Geng,[1] and Tuobing Gou[1]

[1]*Exploration and Development Research Institute of TuHa Oilfield Company, CNPC, Hami, China*
[2]*Key Laboratory of Tectonics and Petroleum Resources, (China University of Geosciences), China*

Correspondence should be addressed to Zhengyin Tang; 1632512357@qq.com

Received 19 January 2022; Accepted 17 February 2022; Published 12 March 2022

Academic Editor: Andrea Brogi

The Ss oil field is found in the Turpan-Hami Basin's Taipei Sag's arc structural belt. This reservoir has a complicated character that has a significant impact on reservoir modeling and production prediction. This is a fault-block reservoir with ultralow permeability and low porosity that is divided by 57 faults. A static model was constructed by Petrel software based on reinterpretation of original log and core data and seismic information so as to clarify the spatial distribution of oil and water in the reservoir and to fit the development history of the later simulated reservoir. The integrated geological modeling approach is described in this work using the Ss reservoir as an example. A 3D structural model was built based on the spatial cutting relationship between the layer model and the fault, and the model's quality was improved by breakpoint data, which more correctly depicted the structural properties of the research area. The lithofacies model was built within the restrictions of sedimentary facies using the sequential Gaussian simulation (SGS) stochastic modeling approach, which is paired with variogram data analysis to achieve the range value. To obtain the porosity and permeability model, the empirical formula of porosity and permeability, the SGS method, and the variation range value was input into the lithofacies model. It is important to note that the input lithofacies and property models have values of the same range. To gain the water saturation model, the distinct S_w function formulas of the $S1 \sim S4$ layer derived from the $J(S_w)$ function were fed into the software. The NTG model was created according to the lower limit of porosity, which is 11%. The merging of detailed reservoir description and simulation led to the establishment of the Ss reservoir geological model. In the plane, the scale of the geological model has reached the meter level and decimeter level in the longitudinal direction. It also offers a framework for optimum reservoir modeling for complex fault-block reservoirs. This method improves the accuracy and precision of the model by reflecting the reservoir's heterogeneity and the oil-water distribution. It could provide more details for future reservoir research such as fine reservoir simulation.

1. Introduction

Fault-block oil and gas reservoirs are intricate and trapped reservoirs produced by fault [1]. Faults are a vital part in fault-block reservoirs, as faults regulate the majority of the reservoir's main attributes [2, 3]. Many faults of various grades, orientations, periods, and mechanical qualities occur in the oil field, cutting and fracturing the structure to produce smaller fault-blocks, which are made up of fault-block groups of various forms and genesis [4]. Reservoir heterogeneity, poor connectivity, substantial lateral shifts, and complex fluid connections are all hallmarks of fault-block reservoirs. Recent studies have shown that faults and their structures have important effects on fluid distribution and reservoir permeability.

Faults are the fundamental building blocks of fault-block reservoirs. Many researchers already have relevant knowledge for studying the fault structure. Based on extensive research using mine practice and laboratory methods, Liotta et al. [5] believe that when the structure interacts with the fault, the axial permeability of the fault increases locally, allowing formation fluids to migrate. Siler et al. [6] simulated

fault slip and historical stress transfer, and they said that stress changes caused by fault slip are important for determining the permeability enhancement and the size of structural discontinuities. According to Brogi et al. [7], faults can act as conduits for formation fluid migration. Smeraglia et al. [8] focused at the active faults in the southern Apennines and thought that the highly permeable fluid conduits were found in the area where the faults fit. Thus, this paper uses a fault-block reservoir composed of fault elements to model 3D geology. The 3D geological modeling research is significant for fluid spatial distribution and seepage studies.

The approach a geological model is created, and scaled-up has a major effect on the simulation grid's final performance, specifically when there is a lot of variability in the reservoir [9]. Fault-block oil and gas reservoirs are more challenging to analyze and classify due to their genesis. Fault-block oil and gas reservoirs are more challenging to analyze and recognize due to their construction [10]. For reservoir geological modeling, determining how to properly and effectively characterize the spatial distribution characteristics of each fault is a complex process.

The ultimate purpose of the geological model's creation is to provide reservoir simulation services. The geological model was established with extensive geological data such as reservoir seismic, well logging, and core, and the generated grid finely illustrates the reservoir's geological properties. In fact, the simulated grid was typically coarsed cell of reservoir flow characteristics with flow unit characteristics [9–11]. As a result, once the geological model is mostly complete, the constructed grid must be coarsened before it can be imported into the simulator.

At present, most research on geological modeling is limited to conventional oil reservoirs, with few introductions to integrated fault-block reservoirs of a case study [12–16]. The Ss reservoir is a low-amplitude dome anticline reservoir dominated by sedimentary facies from the fan delta and braided river delta. The primary oil-producing formations are the Upper Qiketai J2q sand units and the Lower Sanjianfang J2s sand units. It is buried at a depth of 2800-3200 meters, with the water-oil contact at the depth of -2500 meters (shown in Figure 1). Porosity is 12.5%, and permeability is 6.2 mD. The viscosity and density of formation crude oil are 0.39 mPa·s and 0.66 g/cm^3, respectively. The geological model was accomplished in this study after within most latest geological information and development data of the study area, which supplied some reference concepts for later similar research on fault-block oil and gas reserves. Furthermore, it represents research methods for the block's remaining oil development in the future. The study is related to a range of dynamic and static geological data from the Ss reservoir, including seismic, logging, and core analysis, as well as a detailed summary of the work area. Petrel software was utilized to do this geological modeling workflow in the area when combined with detailed geological data. Quantitatively expose the 3D distribution of lithology and facial attributes of reservoirs in the Ss reservoir, as well as the distribution and favorable regions of reserve, in the modeling system.

The first chapter of the study discusses the current understanding about fault-block reservoirs in geologic modeling. The study area's history and geological setting are detailed in the second part. The third section is a quick overview of modeling methodological approach. The fourth and fifth parts present the results of the geological modeling, as well as comments and conclusions.

2. Geological Setting and Study Area

2.1. Location and Development. The Ss reservoir is located in the Taipei Sag of the Turpan-Hami Basin, with Qiuling reservoir to the west and Wenmi reservoir to the east, in the arc structural belt. The reservoir was discovered in the 1950s, but development did not begin until the late 1980s, and production began in the early 1990s [17]. Figure 2 depicts total oil production, total fluid production, and total water content over period.

2.2. Geologic Structure. The Ss structure is a short-axis northwest-trending anticline with a long axis of 9.15 kilometres a short axis of 5.2 kilometres [17, 18]. The reservoir has a closed range of 328.5 meters, a closed area of 38.0 kilometres, and 57 faults. The overall terrain of Ss reservoir is higher in the north and lower in the south, with a small uplift and a nose-like structure in the middle that gradually descends to the two flanks. Figure 3 depicts the recognition of seismic attribute slices such as coherent body, ant body, and tectonic steering filter, as well as how the interpretation results are used to estimate the study area's fault distribution characteristics. Finally, the investigated area's fault structure distribution is confirmed (shown in Figure 4).

2.3. Layered. The primary oil-producing formations are the Upper Qiketai J2q sand units and the Lower Sanjianfang J2s sand units, with an oil layer depth of 2800 m to 3200 m. The J2s of the Sanjianfang formation are divided into oil group SI and SII, applying sequence stratigraphic analysis method and the short-term base level cycle [19]. According to the sedimentary rhythm and lithological variation surface, SI oil group is sorted into S_1 and S_2 sand units, and SII is sorted intoS_3, S_4, and S_5 sand units. Each sand unit is divided into single layer sand for modeling and research purposes, with the specific division results be provided in Table 1. The oil units Q1 are 56.3 meters thick, SI is 105.8 meters thick, and SII is 178 meters thick. In the study area, the productive layer's original oil saturation ranges from 58 to 68.5 percent.

2.4. Porosity and Permeability. In the study area, in-layer heterogeneity is not obvious but the interlayer heterogeneity is very strong [20]. The majority of pore types are secondary. The results of the test suggest that the reservoir rocks have a high degree of hydrophilicity from 14 cores wettability, which is advantageous for water injection development and enhanced oil recovery. The laboratory measured relative permeability curves and normalized them to generate three rock type curves using 33 sample cores with various permeability levels (Figure 5). The Sanjianfang formation's mean permeability and porosity were proved to be 6 mD and

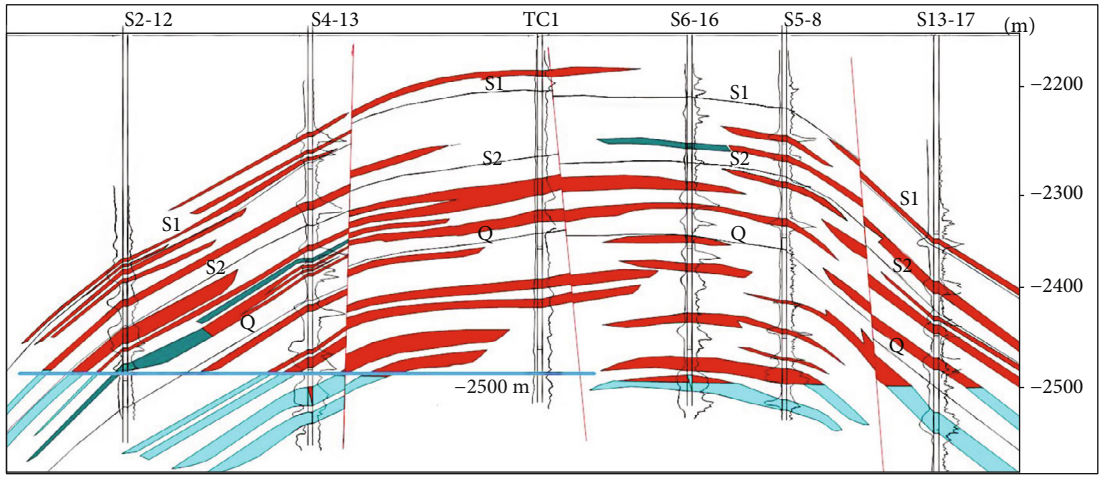

Figure 1: Geological structure of Ss reservoir.

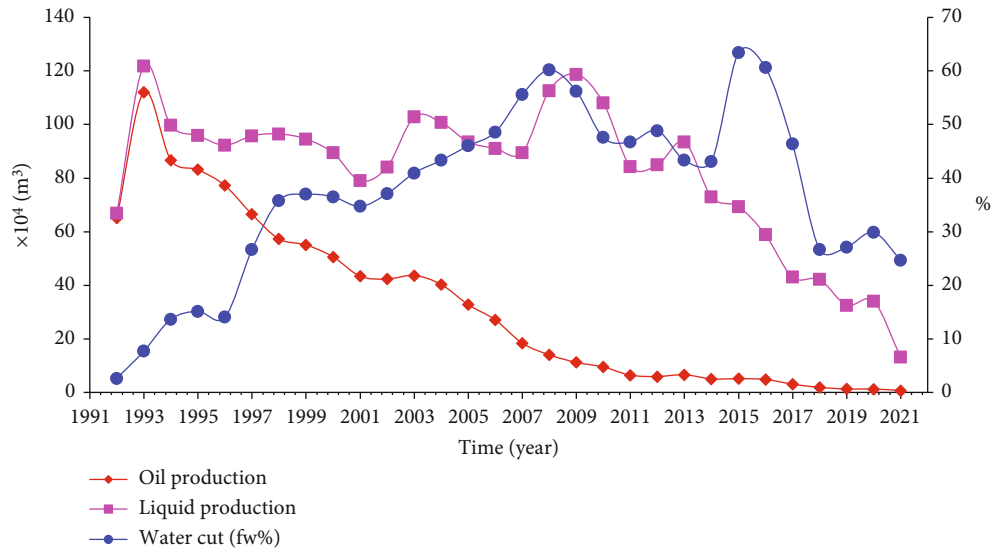

Figure 2: The Ss historical production.

13%, respectively, as shown in Figure 6. The reservoir is characterized by low porosity and ultralow permeability.

2.5. Fluid Properties. Table 2 shows the general fluid properties under initial reservoir conditions as well as the simulation's initialization parameters. The light density, low viscosity, and substantial gas content of crude oil account for its properties [17]. The reservoir has a low associated methane content, but a significant intermediate hydrocarbon ($C_2 \sim C_5$) content. The salinity of the formation water is not high; the water type is $NaHCO_3$ and $CaCl_2$, with $NaHCO_3$ having a salinity of 2000~5000 ppm and $CaCl_2$ having a salinity of 10000~22000 ppm. The initial reservoir pressure is 28.8 MPa, and the pressure coefficient is 0.97, indicating a normal pressure system. The saturation pressure is 18.2 MPa, the reservoir temperature is 86°C, and the geothermal gradient is 2.5°C/100 m, as a low temperature negative anomaly system (the normal geothermal gradient is 3°C/100 m).

3. Materials and Methods

The reservoir geological model is the quantitative expression of diverse geological properties in 3D space and the integration of comprehensive geological research results [21]. As demonstrated in Figure 7, geological modeling necessitates a comprehensive set of a framework. Applying Petrel of 3D modeling software, to make a fault and structural model, facies-controlled model, and property model based on all available geological study results.

Deterministic and stochastic reservoir modeling is the two most commonly used methodologies for reservoir modeling [22–24]. Linear interpolation, inverse square weighted average of distance, kriging method, and seismic

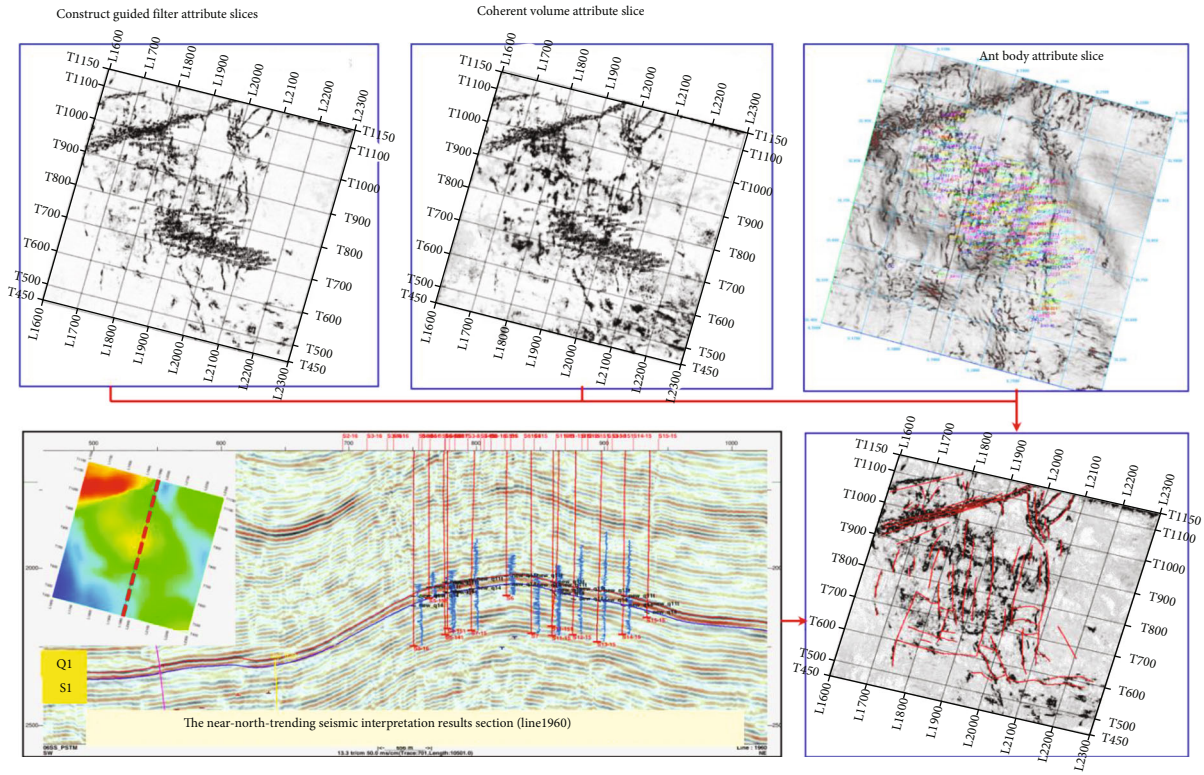

Figure 3: Fault combination and fault system interpretation.

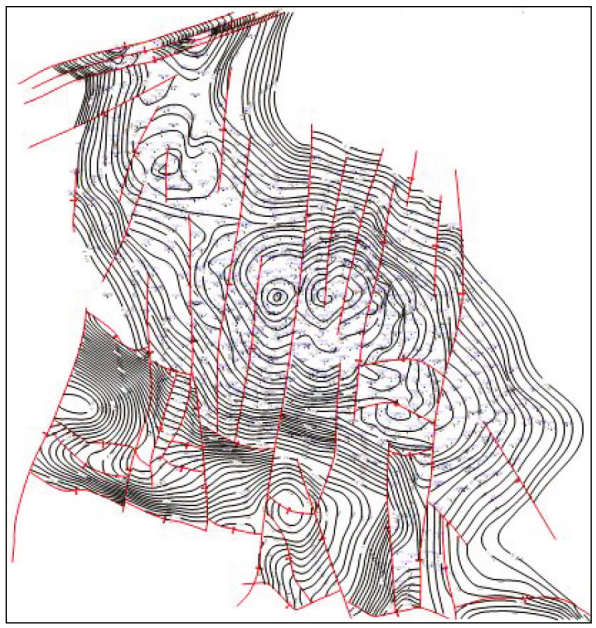

Figure 4: The structure of the study area.

reservoir prediction are among the techniques used in deterministic modeling [25]. The deterministic modeling method is distinguished by the fact that only one output can be obtained by entering a set of parameters. The Kriging interpolation approach may reflect the variogram properties of sand formations of various derivation; however, it is overburdened when dealing with complex fault-block reservoirs.

Table 1: Sand layer division of Ss reservoir.

Oily section	Oil group	Sand units	Single layer units
J_2q	Q_1	Q_1	4
J_2s	S I	S_1	3
		S_2	5
	S II	S_3	5
		S_4	3
		S_5	4
Total	3	6	24

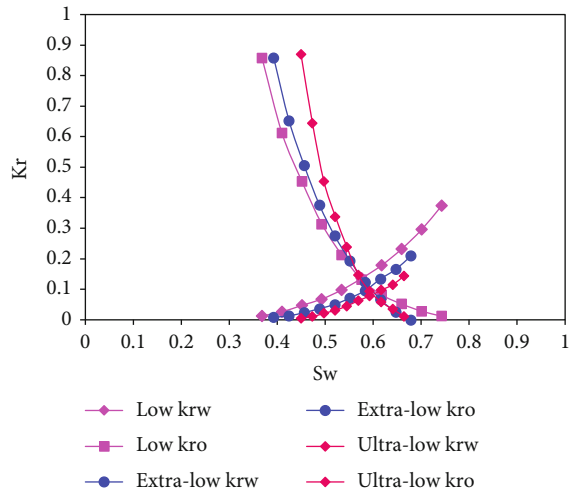

Figure 5: Relative permeability curves of three types.

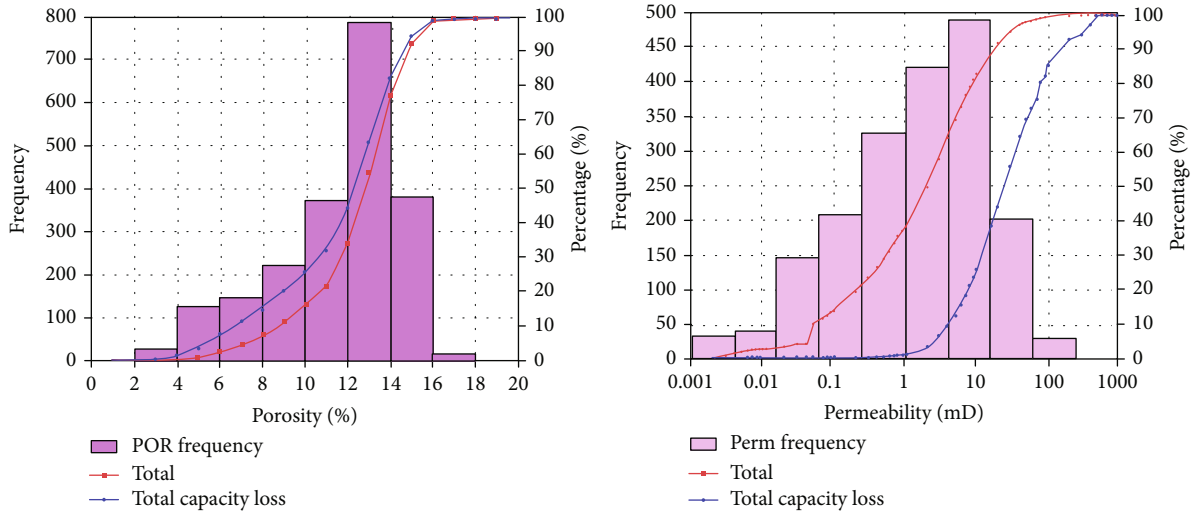

Figure 6: Histogram of porosity (a) and permeability (b) distribution.

Table 2: General fluid properties at initial reservoir conditions and initialization parameters used in the modeling.

Parameter	Value
Oil density	0.6597 g/cm^3
Oil viscosity	0.3879 mPa·s
Oil bubble point pressure	18.2186 MPa
Oil compression factor(co)	16.7486×10^{-4} MPa^{-1}
Gas density	1.04 kg/m^3
Water formation	$NaHCO_3$,$CaCl_2$
Water viscosity	0.3246 mPa·s
Reservoir pressure	28.84 MPa
Reservoir temperature	86°C
Geothermal gradient	2.5 °C/100 m
Depth of water-oil contact	-2500 m

The application of stochastic simulation technology to establish multiple alternative reservoir space parameter forecasts with equal probability of reservoir spatial distribution models is based on known information together with random function theory [26, 27]. Multiple stochastic results generated using the stochastic simulation method can better capture the varied nature of reservoir attribute spatial distribution [28]. Advanced stochastic modeling methods and facies-controlled modeling approaches are needed to construct geological models based on the research objective, depth, and accuracy requirements of the study area.

The fault model is a three-dimensional fault plane that is based on seismic interpretation and fault data to determine fault distribution in space [29]. The layer structure model uses the interpolation method and layered data to build the top and bottom surface models of each isochronous layer [30]. The layer model is a three-dimensional representation of the stratum interface. After merging the space of each layer model, the constructed fault model can be loaded to acquire the reservoir's 3D spatial framework.

Stochastic modeling simulation requires two types of parameters. The conditional parameter is the original geological information. The other category is statistical characteristic parameters, which comprise lithology index variation coefficient, petrophysical variation function, and probability density function [31]. The most advanced method currently used to determine these values is variogram analysis with stratigraphic comparison.

The variogram quantifies the spatial variability of regionalized variables. It reflects the fact that the degree of spatial variability varies with distance and direction. It builds a corresponding theoretical variogram model using limited spatial observations of regionalized variables to reveal the variable's main structural characteristics [31]. Taking the lithofacy interpretation data on the well point as the control point, the horizontal and vertical variation functions of the five lithologic facies of the 24 single sand layers were analyzed, and the variable gradient function model curves were fitted so that various statistical characteristic parameters were relatively well determined, as shown in Table 3. The variogram model curves obtained by analyzing the lateral and vertical variograms of the five lithofacies with the properties of 24 sand layers are depicted in Figure 8.

Following the completion of structural and lithofacies modeling, property modeling, which includes porosity, permeability, water saturation, and NTG models, is performed. Variogram analysis and stochastic modeling method optimization are required in porosity and permeability modeling, as well as when the lithofacies model is established. Accurate modeling of water saturation variation in the transition zone is critical for reservoir simulation and determining original oil in place [32]. There was no complete set of resistivity logs available to generate capillary pressures (P_{cr}) [33]. P_{cHg} data for rock samples were available, which was then converted to the P_{cr} in the following equation.

$$P_{cr} = \frac{\sigma_r \cos\theta_r}{\sigma_l \cos\theta_l} \bullet P_{cHg}, \quad (1)$$

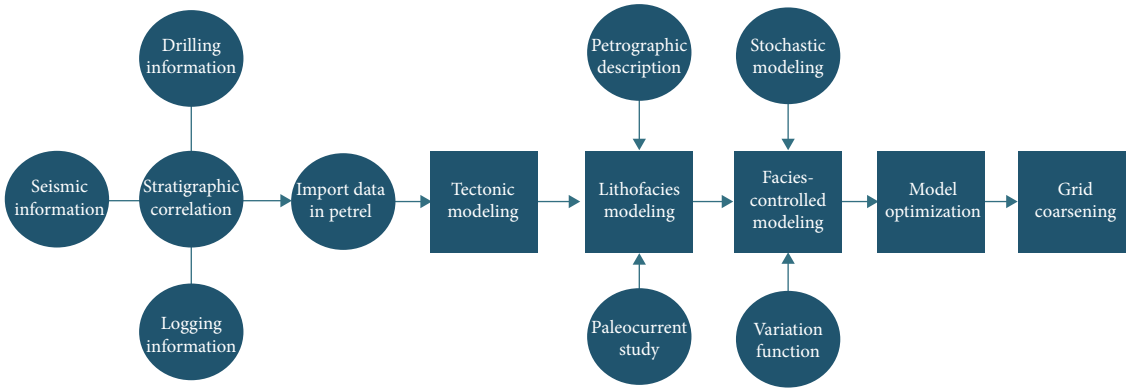

Figure 7: The workflow used for the entire modeling procedure.

Table 3: The variogram fits the input parameter value.

Parameter	Value
Major range	600 meters
Minor range	380meters
Vertical range	3 meters
Major azimuth	SE45°
Vertical dip	90°

where P_{cr} and P_{cHg} are under formation conditions and laboratory conditions capillary pressure (MPa); σ_r and σ_l are the interfacial tension under the formation conditions and laboratory (mN/m); θ_r and θ_l are the capillary angle under the formation and laboratory, respectively. Table 4 provides specific value of the above parameters.

Because of the large density differences between oil and gas and the lack of an initial gas cap in the reservoir, the capillary pressure between them was ignored. Equation (2) was used to convert the obtained capillary pressure data to depth:

$$H = H_O - H_{FWL} = \frac{100P_{cr}}{\rho_w - \rho_o}, \tag{2}$$

where H is the height of oil, m; H_{FWL} is height above the free water level, m; ρ_w is water density, g/cm^3; and ρ_o is oil density, g/cm^3.

Finally, eq. (3) [34, 35] is used to transform the capillary pressure curve under oil reservoir circumstances to the J function in consistent units:

$$J(S_W) = \frac{P_{cr}}{\sigma_r \cos\theta_r} \bullet \sqrt{\frac{k}{\phi}}, \tag{3}$$

where K is permeability (md); ϕ is fractional porosity, %.

Figure 9 shows water saturation and capillary pressure curves for multiple rock samples from S1 to S4.

Data preparation is essential before the modeling work begins. 502 well position and well trajectory data were sorted by the researchers. Fine geological stratification data, logging interpretation curves, seismic tectonic surface and fault data, lithology curves, paleo-current direction data, and other information are also included. Various test data (such as oil test and production data), fluid property data, and production dynamic data must also be prepared.

An orthogonal grid system was used to establish the model grid in the study area. The grid step length is 20 meters on the 2D surface, and a total of 348 × 345 grids are divided. With an average step length of 0.2 meters, it approaches the decimeter level in the longitudinal direction. As a result, a total of 1730 microlayers are separated longitudinally from the upper of the Q sand group to the lower of the S5 sand group, resulting in a total of 348 × 345 × 1730 cells in the 3D modeling. The total number of cells exceeds 200 million. Because the geological model is so detailed, it cannot be directly loaded into the simulator for simulation testing. On the one hand, machine capacity and computer power are significant challenges; on the other hand, they are insignificant for research simulation. As a result, work on coarsening the cell is also required. To check for invalid cells, cell height and volume models were constructed after coarsening the cell of the geological model.

4. Results and Discussion

4.1. Fault Modeling. The fault model is a 3D fault plane that is based on seismic interpretation and fault data to determine fault distribution in space. The layer structure model uses the interpolation method and layered data to build the top and bottom surface models of each isochronous layer. The layer model is a 3D representation of the stratum interface. After superimposing the space of each layer model, the constructed fault model can be loaded to acquire the reservoir's 3D spatial framework.

According to the result of the seismic investigation and interpretation, the study area has 57 faults of various magnitude, with a rather basic fault structure. Applying seismically interpreted fault data to construct each fault plane and analyze the contact and cutting relationships between the faults, a fault model for the entire oil area of the Ss was established, as shown in Figure 10.

4.2. Structural Modeling. From the upper Q to the lower S5 sand, the geological stratification of the study area is divided into 6 layer units and 24 small strata. Although well

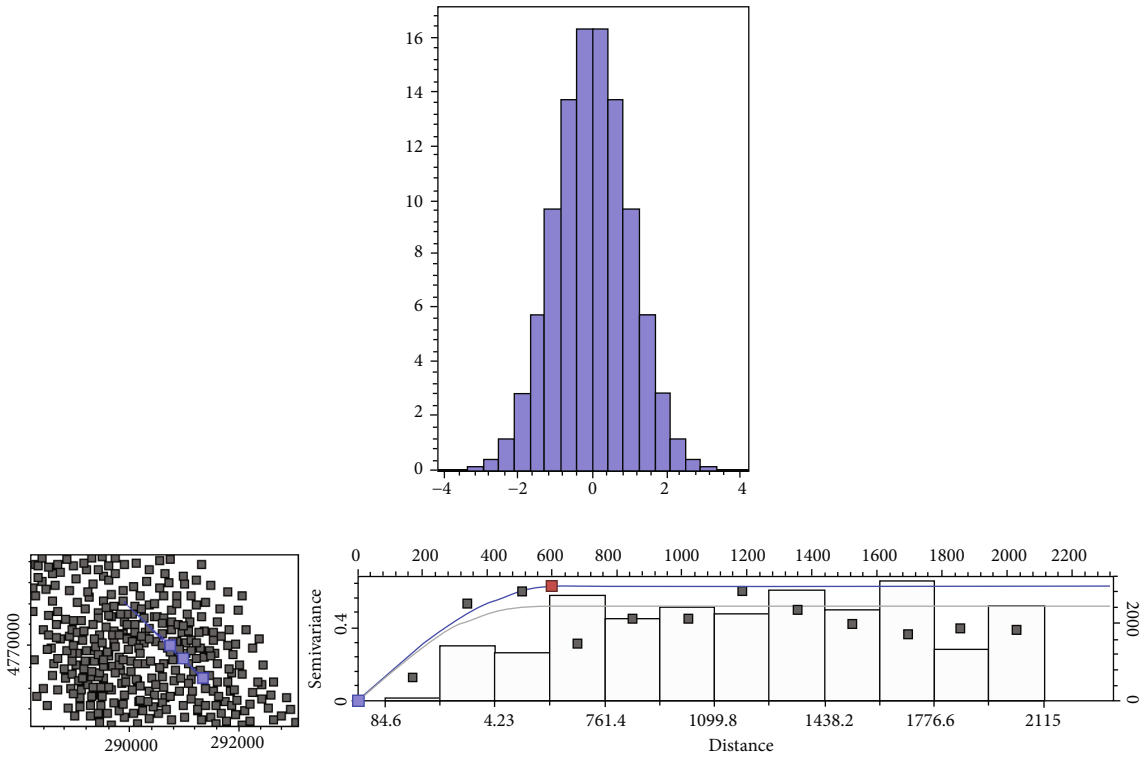

Figure 8: Normalization and matching in variogram analysis.

Table 4: Wetting angle and interfacial tension value [34, 35].

Environment	System	Capillary angle θ (°)	Interfacial tension σ $(\mathrm{mN}m^{-1})$
Laboratory	Gas-water	0	72
	Oil-water	30	48
	Gas-mercury	140	480
	Gas-oil	0	24
Formation	Water-oil	30	30
	Water-gas	0	50

geological stratification data is quite reliable, predicting the value obtained between wells is problematic. Four tiers of upper and lower oil groups were developed based on the interpretation surface data of seismic interpretation in the study (Figure 11) in order to make the structure correspond to the details of wells and reflect the overall trend of seismic interpretation. The four layers were adjusted and reconstructed using the layered data from 502 wells, and the layered thickness surface of 24 single sand layers was established. Finally, a 3D structural model of the Ss was created by merging four layer models, layered thickness planes, and fault models (Figure 12).

4.3. Lithofacies Modeling. The sandstone is categorized into four lithofacies by studying the sedimentary facies of the Ss reservoir: glutenite, medium to coarse sandstone, packsand, and siltstone. To create a 3D lithofacies model, the paper used a combination of stratigraphic lithology and stratigraphic contrast division, log facies analysis, and lithofacies curve interpretation in the study area, as well as paleocurrent direction and advanced stochastic modeling technologies.

The stochastic modeling approach was screened based on variogram analysis, employing logging interpretation of lithofacies data at the well locations as hard information, and a more suitable sequential inertia indicator method was applied to construct 24 layers of 3D lithofacies model. The lithofacies model of the study region is displayed in 3D in Figure 13, and the lithofacies model of the s_2^3 layer is shown in Figure 14.

4.4. Property Modeling. The 3D facies model is used to model the petrophysical parameters. Under the control of conditional wells, statistically evaluate parameters of the standard deviation, probability distribution, and variogram in the facies model, using sequential Gaussian simulation (SGS) to produce the requisite 3D parameter model. The

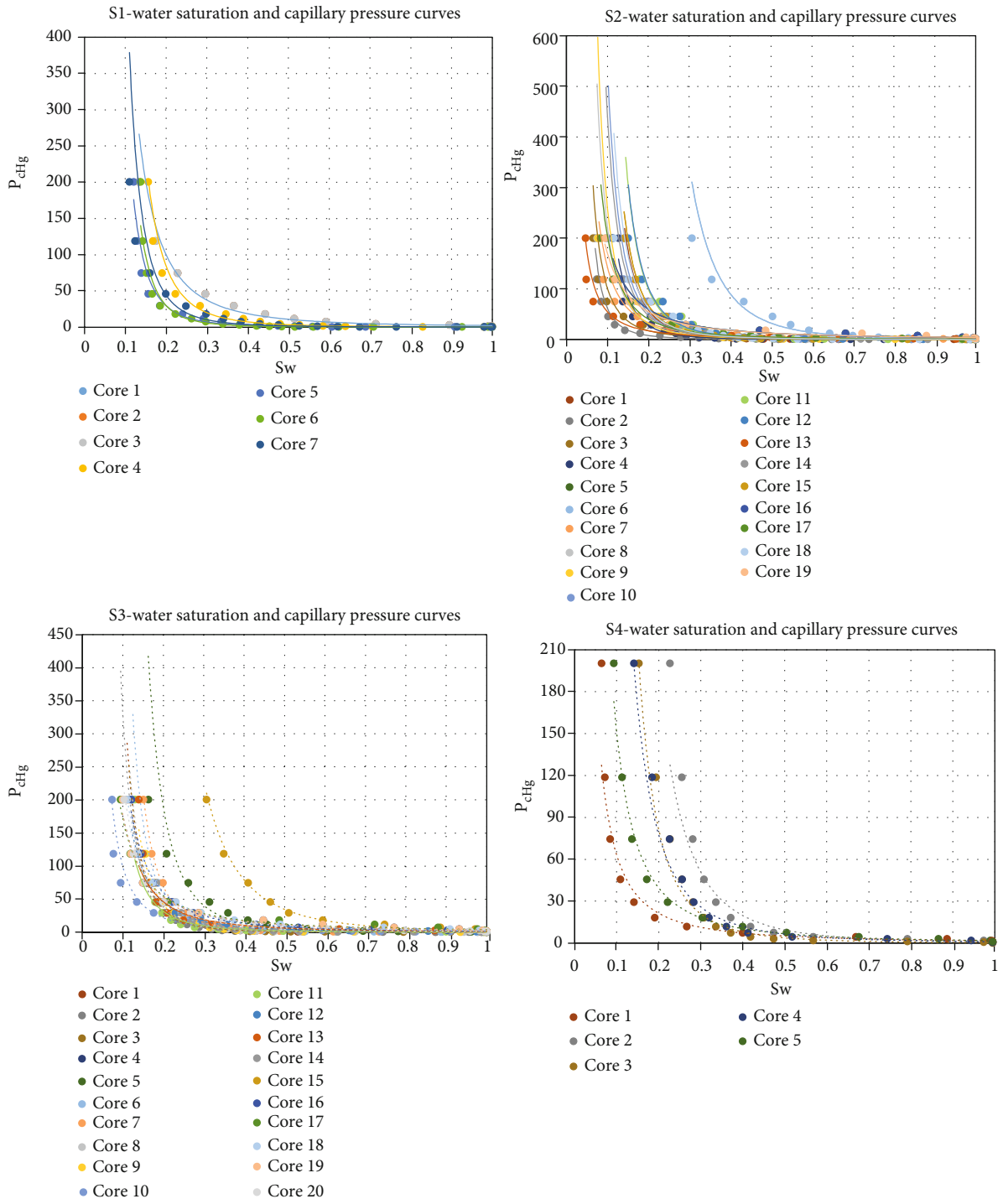

Figure 9: S1 to S4 water saturation and capillary pressure curves.

SGS [36] algorithm provides two benefits. It is first carried out in a sequential manner from one pixel to the next. Second, in addition to the original data, the conditional data utilized to build the conditional probability distribution function of a pixel includes all simulated data.

The porosity is the fundamental parameter that reveals the reservoir capacity's relative size. Porosity accuracy is directly related to the precision of key metrics such as saturation, which is critical in the appraisal and computation of reservoir reserves. The link Eq. (4) between AC and porosity was established using core analysis porosity and logging electrical parameters of the core layer. The relationship between AC and formation porosity is shown in Figure 15(a).

$$\Phi_C = 0.001811 \times AC - 0.2964\left(R^2 = 0.832\, N = 97\right), \quad (4)$$

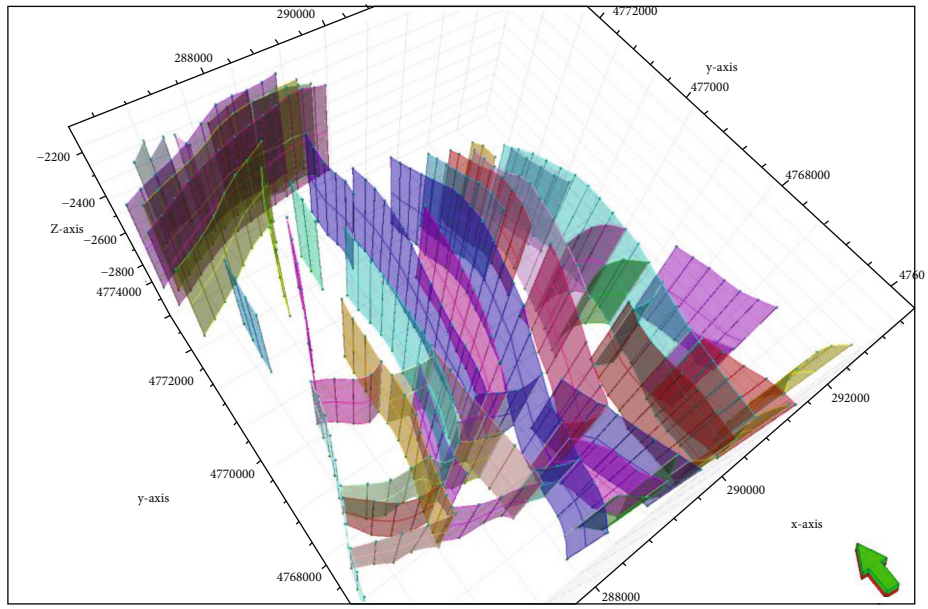

Figure 10: Fault model of the study area.

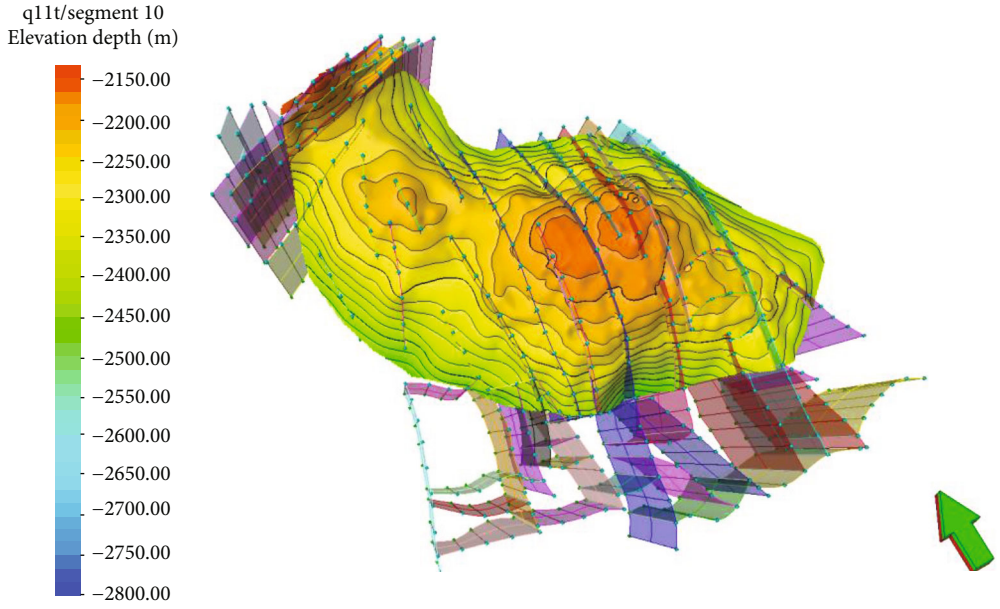

Figure 11: Top structure of the study area.

Where Φ_C is the porosity, AC is the acoustic time difference.

As demonstrated in Figure 15(b), permeability and porosity have a particular relationship. An empirical Eq. (5) for the intersecting permeability of the porosity and permeability of the Ss reservoir is established based on the porosity and permeability data from the core analysis in the research region.

$$K = 0.01097 \times e^{(0.4356 \times \Phi)} \quad \left(R^2 = 0.8039\, N = 139\right), \tag{5}$$

where K is the permeability of reservoir, and Φ is the porosity.

The porosity of mudstone is zero, according to the lithofacies model, when Eq. (4) is used to compute the porosity of sandstone. Discretize the calculated porosity into a property while also setting the porosity of the mudstone and interlayer to low-value ranges of 0 ~ 001. The porosity of sands was distributed according to the real data range, which was combined with the log interpretation of the property parameter data of wells point as the hard data, and 24 layers of 3D porosity models were built using the SGS technique (shown

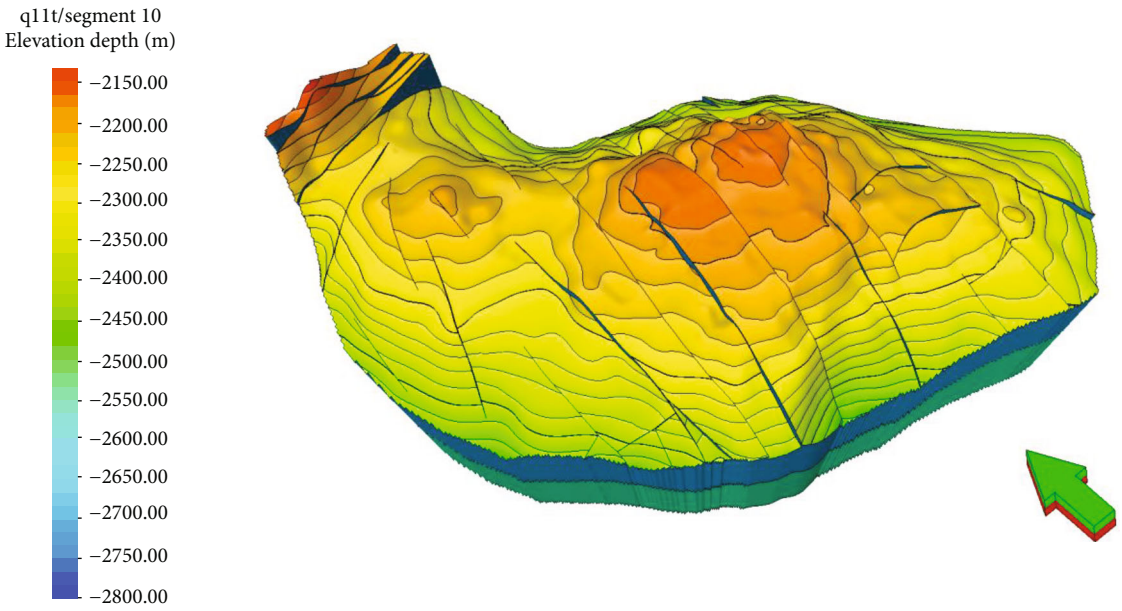

Figure 12: 3D structural model of the study area.

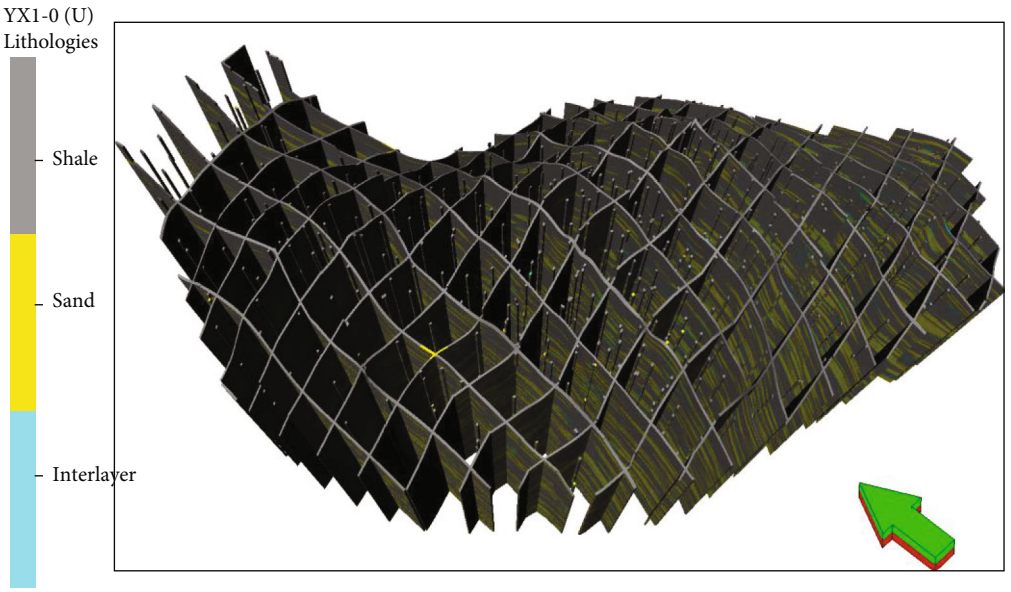

Figure 13: 3D lithofacies model of the study area.

in Figure 16(a)). Given the link between permeability and porosity, developing permeability models is consistent with the above strategy (shown in Figure 16(b)). The longitudinal porosity and permeability model distributions are shown in Figures 16(c) and 16(d), respectively.

Water saturation was computed in every cell of the 3D grid using the height above free water level concept, which was modeled using capillary pressure curves assigned to each reservoir rock type (RRT) in this study. Reservoir rock cores were investigated, and the relationship between capillary force and water saturation (S1 to S4) was determined under experimental settings, as shown in Figure 9. The $J(S_w)$ function and water saturation model (S_w) of (S1 ~ S4) sand units are shown in Table 5. The following is a more detailed explanation of the approach. To begin, Eq. (1) converts the capillary force value measured under experimental conditions into the equivalent value under formation conditions. Second, Eq. (3) was implemented to create a series of J (S_w) values, and then multiple regression matching was used to determine the relationship between J (S_w) and (S_w). Finally,

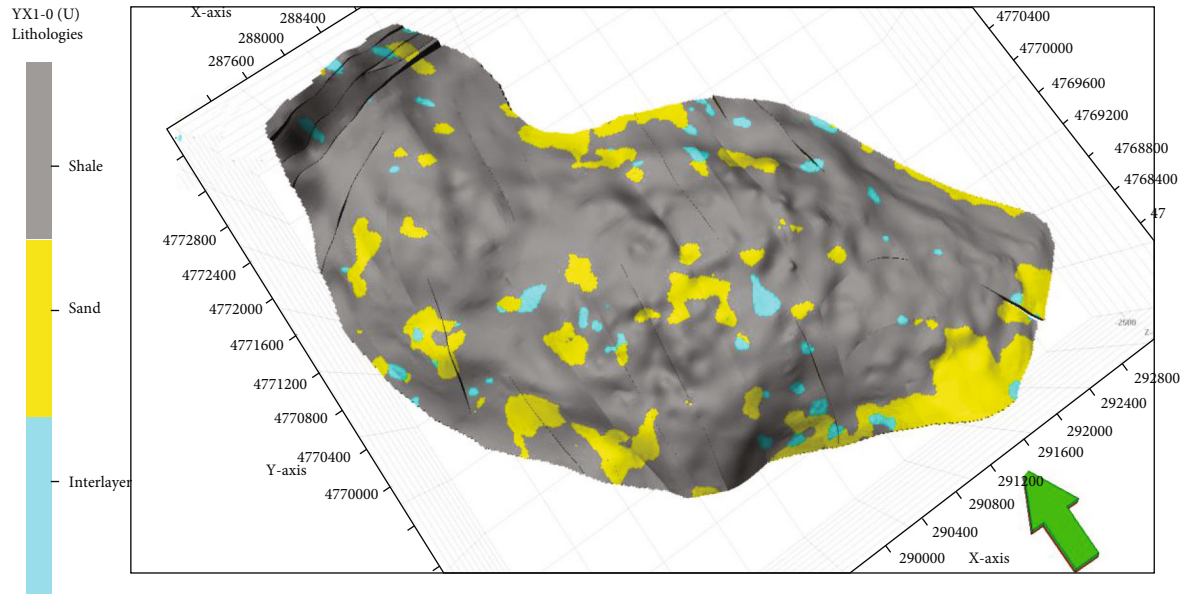

Figure 14: Lithofacies model of s_2^3 layer in the study area.

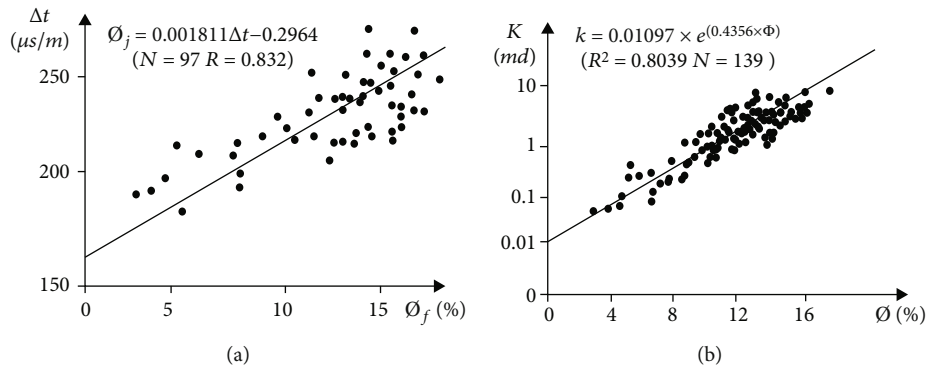

Figure 15: Relation of AC and porosity (a) and relation of permeability and porosity (b).

by integrating Eqs. (2) and (3), the (S_w) function is obtained, which shows the relation between water saturation, formation porosity and permeability, and oil column height of distinct oil layer units. To establish the water saturation model, the derived (S_w) functional relationship was entered into Petrel modeling software. Exhibition of modeled longitudinal cross-sections (S1 to S4) of the water saturation models in primary reservoir regions is shown in Figure 17.

This method improved the petrophysical model's accuracy. When compared to the Archie technique, the calculation accuracy of the water saturation model derived by solving the different levels is greatly improved, and it can disclose the change in saturation near the oil-water interface.

Furthermore, as compared to the simple assignment method's water saturation model, the S_w function model can better expose the original reservoir saturation and give a solid foundation for simulation.

4.5. Net to Gross Modeling. The term "cut-off" refers to a collaborative effort by geological researchers to determine a value that will distinguish non-reservoir rock (mudstone) from reservoir rock [11]. The NTG defines the effective to rock thickness ratio of the reservoir [37]. In this study, geological reserve prove only related to porosity, hence, NTG is primarily controlled by the lower limit of porosity. The intersection diagram of porosity and permeability of Ss reservoir (Figure 18), the lower limit of porosity as $\varnothing_0$ is 11%. The syntax in the model is NTG = if (Por≥11%, 1, 0). Figure 19 illustrates the NTG model of S_2^3.

4.6. Calculation of Reserves. The calculation of geological reserves is an initial test of the model's quality after it has been established. The thorough results of the initial geological model reserve calculation for the study area are shown in Table 6. The calculated reserves of the initially geological model are 3969×10^4 m^3, which is 3.5% deviation than the

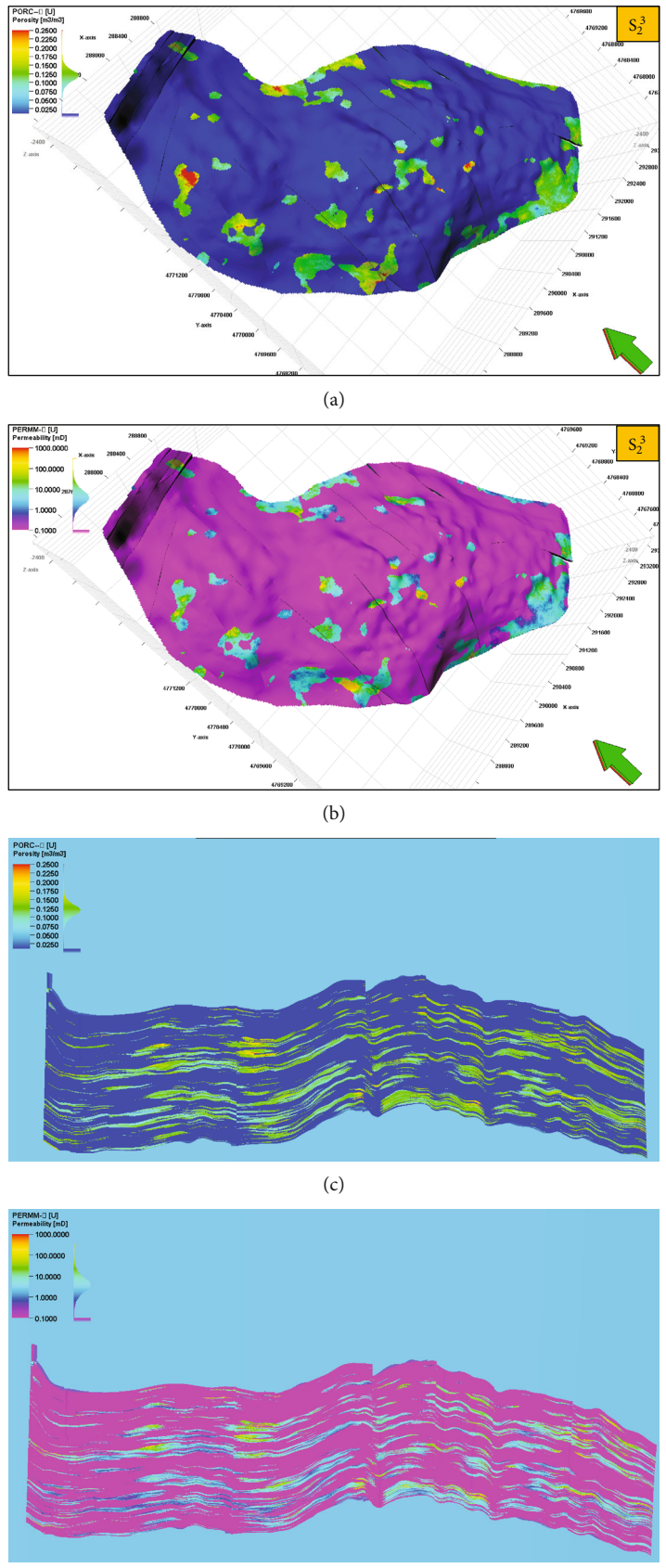

FIGURE 16: Porosity (a) and permeability (b) model of s_2^3 layer, longitudinal section of the porosity (c) and permeability (d) model.

Table 5: (S_w) and $J\ (S_w)$ function of (S1 ~ S4) sand units.

Sand units	J-function ($J\ (S_w)$)	(S_w) function
S1	$J\ (S_w) = 0.0838 \times S_w^{-3.3} R^2 = 0.8951$	$S_w = 1.1206638\left(\frac{1}{h} \times \sqrt{\frac{\varnothing}{k}}\right)^{\frac{1}{3.445}}$
S2	$J\ (S_w) = 0.0968 \times S_w^{-2.648} R^2 = 0.7405$	$S_w = 1.287414\left(\frac{1}{h} \times \sqrt{\frac{\varnothing}{k}}\right)^{\frac{1}{2.719}}$
S3	$J\ (S_w) = 0.1247 \times S_w^{-2.692} R^2 = 0.7315$	$S_w = 1.294725\left(\frac{1}{h} \times \sqrt{\frac{\varnothing}{k}}\right)^{\frac{1}{2.496}}$
S4	$J\ (S_w) = 0.3421 \times S_w^{-2.146} R^2 = 0.8768$	$S_w = 1.295409\left(\frac{1}{h} \times \sqrt{\frac{\varnothing}{k}}\right)^{\frac{1}{2.56}}$

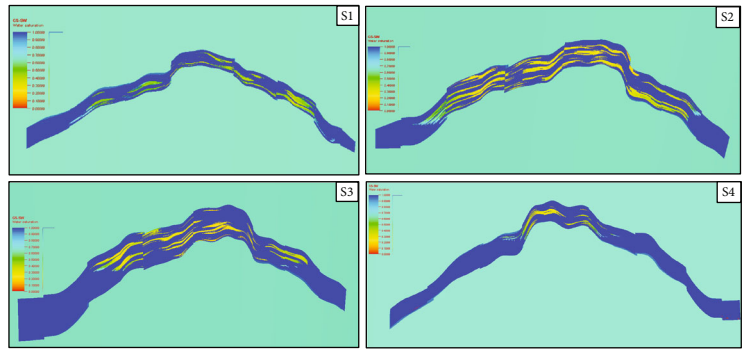

Figure 17: Longitudinal cross-sections of the S1 ~ S4 water saturation models.

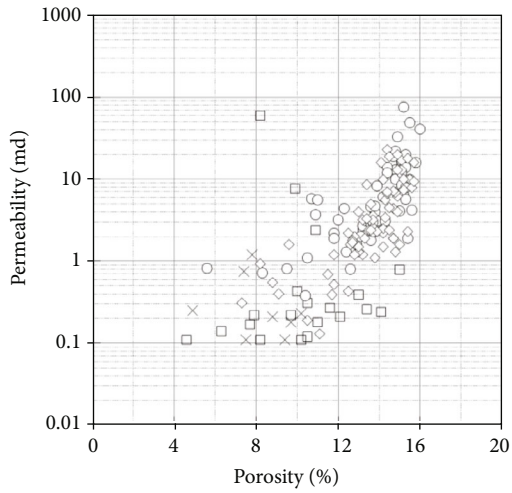

Figure 18: Intersection diagram of porosity and permeability.

geological reserves of $4114 \times 10^4\ m^3$, which conform the error range of model requirements.

4.7. Model Coarsening. The geological modeling work is nearly complete now that the structural, lithofacies, and property models have been completed. The goal of finishing the modeling work is to make a proper support structure for simulation. The lithofacies model, porosity model, and permeability model were coarsened in order to allow the geological model to be entered into the simulator to finish the simulation study work. The coarsening process varies based on the qualities of attribute parameters [38].

The geological model was coarsened to allow the output model grids to be appropriate to simulation work and to minimize the process of modifying parameters throughout the simulation process. The vertical distribution frequency of single sand is adopted by the cells coarsening of the lithofacies model. A weighted arithmetic average approach is used to coarsen the porosity and permeability models. The grid step length was coarsened to 50×50 meters on the 2D surface, and a total of 139×138 grids were divided. The 1730 microlayers are coarsened 72 layers in the longitudinal direction through the three small layers of each single sand unit as the boundary coarsening condition. After coarsening, the total number of cells in the output model is $139 \times 138 \times 72$. The stratified reserves are rematched when the model is coarsened. The coarsened model reserve is calculated to be $4121 \times 10^4\ m^3$. The deviation between the simulation results of coarsened model and the geological reserves is only 0.2%. This demonstrates that the model's reserves estimate through grid coarsening is more reasonable than noncoarsening, the coarsened model more appropriate for research.

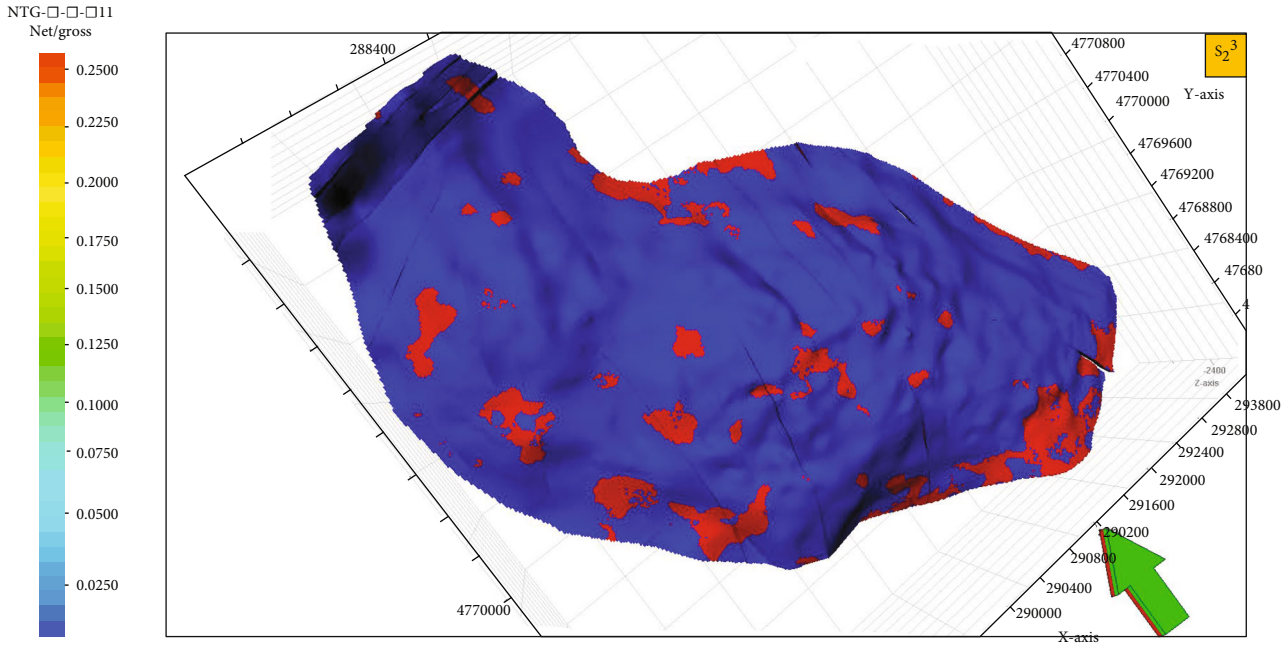

Figure 19: The NTG model of S_2^3.

Table 6: Reserve matching result of Shansan 3D model.

Sand units	Q_1	S_1	S_2	S_3	S_4	S_5	Total
Match reserve $\times 10^4 m^3$	618	879	1495	737	148	88	3969

5. Conclusion

(1) The integration of detailed reservoir description and simulation led to the creation of the Ss reservoir geological model. In the plane, the geological model has reached the meter level, and in the longitudinal direction, it has reached the decimeter level. The grid step length on the 2D surface was 20 meters, and a total of 348×345 grids were separated. In the longitudinal direction, the 1730 microlayers are divided longitudinally from the upper of the Qiketai to the lower of the S5 sand group, and the total number of nodes in the 3D modeling is $348 \times 345 \times 1730$ cells. The 3D model reserves match is $3969 \times 10^4\ m^3$, which is 3.5% deviation than the geological reserves of $4113 \times 10^4\ m^3$. The results show that the model meets the accuracy and research purpose requirements

(2) Advanced stochastic simulation methods are used to solve the complex fault-block model, which visually displays the spatial distribution characteristics of the reservoir and improves the fine description of the reservoir, as part of reservoir modeling research that closely combines the formation and sand body distribution characteristics of the Ss reservoir. This gives a parametric model for simulation due to its precision. The properties of complicated fault-block reservoir are extremely important to research

(3) The study not only offers fault-block reservoir modeling approaches but it also publishes a vast number of geological data bodies in the study region, including 430 production well history data and reservoir material properties, as well as proposing directions for future geological research.

(4) Through the application of variogram analysis to acquire a great grasp of sand bodies, geological study, lithofacies simulation, and physical parameter simulation become a trinity. The spatial distribution of lithofacies and petrophysical parameters is adequately displayed in lithofacies modeling and property modeling, and geological research and reservoir modeling are closely coupled to make the subsequent simulation results more realistic and dependable.

Data Availability

The oil field geological description, except the information presented in the manuscript, used to support the findings of this study is restricted by the Safety Law of Petrel China. However, other data such as the depth or reservoir fluid description used to support the findings are currently under embargo while the research findings are commercialized. Requests for data, 12 months after publication of this article, will be considered by the corresponding author.

Conflicts of Interest

The author(s) declare(s) that they have no conflicts of interest.

Acknowledgments

The authors thank Tuha Oilfield Research Institute for providing the detailed geological background and date of the reservoir.

References

[1] X. Zhuang and S. Huang, "Establishment of fine 3D geological model of fault-block reservoir," *Application of Petrochemical Industry*, vol. 38, no. 11, pp. 79–82, 2019.

[2] X. Pan, J. Li, L. Zhou, J. Gong, Y. H. Chen, and Q. C. Chen, "Structural modeling of oil and gas reservoirs in complex fault-block groups and its application," *Fault-Block Oil and Gas Fields*, vol. 2008, no. 6, pp. 53-54–53-58, 2018.

[3] D. Jinhu, S. Yi, and Q. Wang, "Exploration practice and understanding of subtle reservoirs in Huabei Oil field," *China Petroleum Exploration*, vol. 2003, no. 1, pp. 1-10–1-15, 2003.

[4] P. Gillespie, T. Skov, and P. La Pointe, "Use of an ant -tracking algorithm for fractured reservoir modeling workflow," in *Conference on Fractured Reservoirs, Geological Society of London Burlington House*, pp. 16-17, London, 2004.

[5] D. Liotta, A. Brogi, G. Ruggieri, and M. Zucchi, "Fossil vs. active geothermal systems: a field and laboratory method to disclose the relationships between geothermal fluid flow and geological structures at depth," *Energies*, vol. 14, no. 4, article 933, 2021.

[6] D. L. Siler, N. H. Hinz, and J. E. Faulds, "Stress concentrations at structural discontinuities in active fault zones in the western United States: implications for permeability and fluid flow in geothermal fields," *Bulletin*, vol. 130, no. 7-8, pp. 1273–1288, 2018.

[7] A. Brogi, M. C. Alcicek, D. Liotta, E. Capezzuoli, M. Zucchi, and P. F. Matera, "Step-over fault zones controlling geothermal fluid-flow and travertine formation (Denizli Basin, Turkey)," *Geothermics*, vol. 89, article 101941, 2021.

[8] L. Smeraglia, A. Giuffrida, S. Grimaldi et al., "Fault-controlled upwelling of low-T hydrothermal fluids tracked by travertines in a fold-and-thrust belt, Monte Alpi, southern apennines, Italy," *Italy. Journal of Structural Geology*, vol. 144, article 104276, 2021.

[9] A. Asadi-Eskandar, H. Rahimpour-Bonab, S. Hejri, K. Afsari, and A. Mardani, "Consistent geological-simulation modeling in carbonate reservoirs, a case study from the Khuff Formation. Persian Gulf," *Journal of Petroleum Science and Engineering*, vol. 109, pp. 260–279, 2013.

[10] B. Lv and Y. Luo, *Bo Wang, et al.*, IOS Press, Natural fractures characteristics of the carboniferous volcanic reservoir in northwestern margin of Junggar Basin, 2021.

[11] I. O. Kohshour, M. Ahmadi, and C. Hanks, "Integrated geologic modeling and reservoir simulation of Umiat: a frozen shallow oil accumulation in national petroleum reserve of Alaska," *Journal of Unconventional Oil and Gas Resources*, vol. 6, pp. 4–27, 2014.

[12] H. E. Zhiliang, S. U. N. Jianfang, G. U. O. Panhong, W. E. I. Hehua, L. Y. U. Xinrui, and H. A. N. Kelong, "Construction of carbonate reservoir knowledge base and its application in fracture-cavity reservoir geological modeling," *Petroleum Exploration and Development*, vol. 48, no. 4, pp. 824–834, 2021.

[13] A. A. Radwan, M. A. Abdelwahhab, B. S. Nabawy, K. H. Mahfouz, and M. S. Ahmed, "Facies analysis-constrained geophysical 3D-static reservoir modeling of Cenomanian units in the Aghar oilfield (Western Desert, Egypt): insights into paleoenvironment and petroleum geology of fluviomarine systems," *Marine and Petroleum Geology*, vol. 136, article 105436, 2022.

[14] J. Zheng, P. A. N. Wenqing, S. H. E. N. Anjiang et al., "Reservoir geological modeling and significance of Cambrian Xiaoerblak Formation in Keping outcrop area, Tarim Basin, NW China," *Tarim Basin, NW China, Petroleum Exploration and Development*, vol. 47, no. 3, pp. 536–547, 2020.

[15] H. V. Thanh, Y. Sugai, R. Nguele, and K. Sasaki, "Integrated workflow in 3D geological model construction for evaluation of CO_2 storage capacity of a fractured basement reservoir in Cuu Long Basin. Vietnam," *International Journal of Greenhouse Gas Control*, vol. 90, article 102826, 2019.

[16] T. A. N. Xuequn, L. I. U. Yunyan, Z. H. O. U. Xiaozhou, L. I. U. Jiandang, R. Zheng, and J. I. A. Chao, "Multi-parameter quantitative assessment of 3D geological models for complex fault-block oil reservoirs," *Petroleum Exploration and Development*, vol. 46, no. 1, pp. 194–204, 2019.

[17] F. Bai, "Study on geological characteristics and development technology of Ss oilfield," *Sinopec*, vol. 11, pp. 39-40, 2017.

[18] Y. C. An, "Reservoir Characteristics of Ss Oilfield," in *Northeast University of Petroleum, China*, Northeast University of Petroleum Press, 2011.

[19] L. Liu, "Small layer correlation of Sanjianfang formation in Ss oilfield, Xinjiang," *Sedimentation and Tethys Geology*, vol. 3, pp. 25–32, 2000.

[20] G. Luo, "Fine Reservoir Description in Ss Oilfield," in *Daqing Petroleum Institute, China*, Daqing Petroleum Institute Press, 2010.

[21] O. Lerat, P. Nivlet, B. Doligez et al., "Construction of a stochastic geological model constrained by high-resolution 3D seismic data-application to the Girassol field, offshore Angola," in *SPE Annual Technical Conference and Exhibition*, Anaheim, California, U.S.A., Nov 2007.

[22] M. Varga, A. Schaaf, and F. Wellmann, "GemPy 1.0: open-source stochastic geological modeling and inversion," *Geoscientific Model Development*, vol. 12, no. 1, pp. 1–32, 2019.

[23] A. Cáceres, X. Emery, L. Aedo, and O. Gálvez, "Stochastic geological modeling using implicit boundary simulation," in *Proceedings of the 2nd International Seminar on Geology for the Mining Industry GEOMIN*, p. 21, Antofagasta, Chile, 2011.

[24] O. Rashad, A. N. El-Barkooky, A. El-Araby, and M. El-Tonbary, "Deterministic and stochastic seismic inversion techniques towards a better prediction for the reservoir distribution in NEAG-2 Field, north Western Desert, Egypt," *Egyptian Journal of Petroleum*, vol. 31, no. 1, pp. 15–23, 2022.

[25] W. B. Zhang, T. Z. Duan, and Y. F. Liu, "Application status and development trend of quantitative geological modeling technology," *Geological Science and Technology Information*, vol. 38, no. 3, pp. 264–275, 2019.

[26] Y. Lin, G. Zhang, M. Huang, and B. Wang, "Stochastic simulation and inversion method based on random medium theory and gradual deformation algorithm," in *SEG/AAPG/SEPM First International Meeting for Applied Geoscience & Energy*, Denver, Colorado, USA, Sep-Oct 2021OnePetro.

[27] G. Latouche and V. Ramaswami, "Introduction to Matrix Analytic Methods in Stochastic Modeling," in *Society for Industrial and Applied Mathematics*, United States, Technometrics, 1999.

[28] M. Finkelstein and J. H. Cha, *Stochastic Modeling for Reliability. Shocks, Burn-in and Heterogeneous Populations. Springer Series in Reliability Engineering*, Springer, London, 2013.

[29] D. J. Andrews, "A stochastic fault model: 1. static case," *Journal of Geophysical Research: Solid Earth*, vol. 85, no. B7, pp. 3867–3877, 1980.

[30] L. Zhu, M. Li, C. Li et al., "Coupled modeling between geological structure fields and property parameter fields in 3D engineering geological space," *Engineering Geology*, vol. 167, pp. 105–116, 2013, (In Chinese).

[31] L. Y. Faust, "A velocity function including lithologic variation," *Geophysics*, vol. 18, no. 2, pp. 271–288, 1953.

[32] S. G. Ghedan, B. M. Thiebot, and D. A. Boyd, "Modeling original water saturation in the transition zone of a carbonate oil reservoir," *SPE Reservoir Evaluation & Engineering*, vol. 9, no. 6, pp. 681–687, 2006.

[33] J. Amyx, M. D. Bass, and L. R. Whiting, *Petroleum Reservoir Engineering Physical Properties*, McGraw-Hill Companies, 1960.

[34] Y. Yongliang, "A method of establishing oil saturation model based on J function," *Journal of Colleges and Universities of Petrochemical Industry*, vol. 27, no. 5, pp. 69–71, 2014.

[35] C. Chen, H. Cai, H. J. Liao, D. W. Qin, B. Chen, and X. Huang, "Geological modeling method of saturation constrained by J function in offshore oil and gas fields," *Petroleum Geology and Engineering*, vol. 30, no. 1, pp. 103–105, 2016.

[36] J. M. Mayer, D. Stead, I. de Bruyn, and M. Nowak, "A sequential Gaussian simulation approach to modelling rock mass heterogeneity," in *48th US Rock Mechanics/Geomechanics Symposium*, Minneapolis, Minnesota, June 2014.

[37] P. H. Widjaja and D. Noeradi, "3D properties modeling to support reservoir characteristics of W-ITB field in Madura Strait area," *Bulletin of the Marine Geology*, vol. 25, no. 2, pp. 77–88, 2016.

[38] M. J. King, K. S. Burn, P. Wang et al., "Optimal coarsening of 3D reservoir models for flow simulation," *SPE Reservoir Evaluation & Engineering*, vol. 9, no. 4, pp. 317–334, 2006.